DESY 99-167
LC-TH-2000-002
December 1999

Resonant production of heavy MSSM Higgs bosons at the Photon Collider

José I. Illana*

Deutsches Elektronen-Synchrotron DESY,
Platanenallee 6, D-15738 Zeuthen, Germany

Abstract

Assuming a light Higgs boson is discovered, its nature may remain unknown in case that no supersymmetric particles are found. The detection and study of heavier Higgs particles is then of great interest. For this purpose the Compton-collider option of a high energy e^+e^- linear collider is optimal both to produce Higgs bosons and to reveal their CP-parity. Assuming realistic photon luminosities for various configurations of laser and linac polarizations, we study the heavy, neutral MSSM Higgs signals for the most relevant decay modes as well as their corresponding backgrounds. The MSSM H and A Higgs bosons with masses up to a ∼80% of the linac c.m.s. energy may be observed and their CP-parity tested for Higgs masses $\lesssim$ 450 GeV, at the $\gamma\gamma$ mode of a $\lesssim$ 1 TeV linear collider.

*On leave from Departamento de Física Teórica y del Cosmos, Universidad de Granada, Fuentenueva s/n, E-18071 Granada, Spain.
E-mail: `jillana@ifh.de`

1 Introduction

The global fits to electroweak precision observables provide indirect evidence of a relatively light Higgs boson, $M_{H^0} = 76^{+85}_{-47}$ GeV [1]. Its discovery is one of the main goals of present and planned experiments. When such a particle is found it will be of utmost importance to determine its properties, in particular to know whether it corresponds or not to the only Higgs boson of the Standard Model (SM) H^0. Most of the models beyond the SM predict an extended Higgs sector [2]. In the minimal supersymmetric SM (MSSM) [3] one has two Higgs doublets yielding five physical Higgs particles after the spontaneous breaking of the gauge symmetry: two CP-even, neutral Higgs bosons, h, which must be light ($M_h \lesssim 130$ GeV [4]) and H, which can be heavy; one CP-odd, neutral A and two charged Higgses $H^{\pm}$. The current direct searches provide the limits $M_{H^0} > 89.7$ GeV, $M_h > 79.6$ GeV, $M_A > 80.2$ GeV [5].

In case that a light Higgs particle, with mass below ~ 130 GeV, is discovered at LEP 2, Tevatron or at the future LHC or a high energy lepton collider, and no supersymmetric particles are observed, it will have very probably SM-like properties: the same quantum numbers and almost identical decay rates [6]. It is then clear that discriminating SM and MSSM will require either *(i)* the detection of the slight differences between H^0 and h, or *(ii)* the direct observation of heavier Higgs bosons.

For both purposes the photon-collider option of a linear e^+e^- collider [7] has been proven to be optimal [8]. In first place, the best way to discriminate between the SM and the lightest MSSM Higgs particles is to look at the *loop-induced* Higgs boson couplings such as Φgg, $\Phi Z\gamma$ and $\Phi\gamma\gamma$, with $\Phi = H^0$ or h. They are very sensitive to effects from *new physics* and, among them, the last one is the most promising. The measurement of the two-photon width of an intermediate-mass Higgs boson with an accuracy of $\sim 2\%$ is possible [9]. Secondly, the Higgs bosons are produced *resonantly* by the fusion of two photons with invariant masses that can be as large as $\sim 80\%$ of the energy of the e^+e^- collider energy. This means, in general, a higher discovery reach than using e^+e^- or hadron processes at the same energy.

The determination of the CP nature of the Higgs bosons is also an important issue. The photon collider provides the "most elegant way" [2] to determine whether the Higgs field φ is a pure or a CP-mixed state. Since CP-even and CP-odd components couple with similar strength to $\gamma\gamma$ (via one-loop graphs), the CP-odd components are not masked such as occurs in the processes where the $ZZ\varphi$ or $WW\varphi$ couplings are involved.

In this work we pursue possibility *(ii)*. In the context of a photon collider we study the discovery reach and the discrimination power of the CP-parity of the heavy neutral Higgs bosons of the MSSM. The work is organized as follows. The main features of the photon collider are outlined in Section 2. The $\gamma\gamma$ luminosity and the polarization effects are introduced in Section 3. The Higgs-boson phenomenology at the photon collider is presented in Section 4. The event rates for decaying heavy MSSM Higgs bosons and their backgrounds as well as the statistical significances of the signals for the case of circularly polarized lasers are given in Section 5. In

Section 6, linearly polarized lasers are used to distinguish between H and A. Finally the main conclusions are summarized in Section 7.

2 The photon collider

Due to severe synchrotron radiation in storage rings, future e^+e^- colliders in the TeV region will be linear. Unlike the situation in storage rings, in linear colliders each bunch is used only once. This enables to use of electrons or positrons for the production of high energy photons to obtain colliding $\gamma\gamma$ and γe beams [7]. The $e \to \gamma$ conversion mechanism in the photon linear collider (PLC) is the Compton backscattering of electron and laser photos. This mechanism presents advantages over others (bremsstrahlung, beamstrahlung) because of the possibility to obtain high energy real photons, high monochromaticity and a high degree of polarization of backscattered photons (using polarized lasers and electron beams) and good background conditions.

2.1 Spectrum of backscattered photons

The Compton scattering of low energy photons ($\omega_0 \sim 1$ eV) by high energy electrons ($E_b \sim$ 100 GeV) results in a tight bunch of backscattered photons. The kinematics of the process is governed by the dimensionless parameter x_0, defined from $W_{e\gamma}^2 \simeq m_e^2(x_0+1)$, $x_0 \equiv 4\omega_0 E_b/m_e^2$. The maximal energy fraction $y = \omega/E_b$ carried by the backscattered photons is $y_{\max} = x_0/(x_0+1)$ and their scattering angle is $\theta(y) \approx \theta_0\sqrt{y_{\max}/y - 1}$, with $\theta_0 \equiv m_e\sqrt{x_0+1}/E_b$, of the order of a few microradians.

The spectrum of the scattered photons $f_C(y)$ depends on the product of the mean helicity of the initial electrons and the degree of circular polarization of the laser photons, $\boldsymbol{\lambda_e}\mathbf{P_c}$, [10]

$$\frac{\mathrm{d}f_C}{\mathrm{d}y} = \frac{1}{\sigma_C}\frac{\mathrm{d}\sigma_C}{\mathrm{d}y} = \frac{1}{\sigma_C}\frac{2\sigma_0}{x_0}\left[\frac{1}{1-y} + 1 - y - 4r(1-r) - 2\,\boldsymbol{\lambda_e}\mathbf{P_c}\,x_0 r(2r-1)(2-y)\right], \qquad (1)$$

where $\sigma_0 \equiv \pi\alpha^2/m_e^2$, $r \equiv y/x_0(1-y)$ and the total Compton cross-section is

$$\begin{aligned}
\sigma_C &= \sigma_C^{\mathrm{np}} + 2\boldsymbol{\lambda_e}\mathbf{P_c}\,\sigma_p, \\
\sigma_C^{\mathrm{np}} &= \frac{2\sigma_0}{x_0}\left[\left(1 - \frac{4}{x_0} - \frac{8}{x_0^2}\right)\ln(x_0+1) + \frac{1}{2} + \frac{8}{x_0} - \frac{1}{2(x_0+1)^2}\right] \\
\sigma_p &= \frac{2\sigma_0}{x_0}\left[\left(1 + \frac{2}{x_0}\right)\ln(x_0+1) - \frac{5}{2} + \frac{1}{x_0+1} - \frac{1}{2(x_0+1)^2}\right].
\end{aligned} \qquad (2)$$

It is possible to tailor the shape of the energy distribution by selecting a convenient polarization for the colliding electron and laser beams: *flat* distributed scattered photons when laser and electrons have *like-handed* polarization, and quite *monochromatic* scattered photons (peaked at $y_{\max}$) by colliding *opposite-handed* electrons and photons [10]. The monochromaticity of the spectrum improves by increasing the energy of the initial beams, but the annihilation of a laser photon with a high energy backscattered photon into an e^+e^- pair will occur above the threshold for this reaction, $W^2_{\gamma\gamma'} = (\omega_{\max}+\omega_0)^2 - (\omega_{\max}-\omega_0)^2 > 4m_e^2$. Therefore, one generally demands $x_0 \lesssim 2(1+\sqrt{2}) \approx 4.83$ to prevent this unwanted process.

2.2 Two-photon processes

The high energy backscattered photons produced from one electron/positron beam of the linear collider can be brought into collision with similarly produced photons from the other beam, resulting in $\gamma\gamma$ processes.

Because of the small, but non-zero, photon scattering angles, the luminosity distribution depends on the conversion distance (distance from the conversion point, where the laser pulse intersects the electron beam, to the interaction point) and on the size and shape the electron beam would have in the absence of the laser. The effect of a non-zero conversion distance b enters through a geometrical factor $\rho = b\theta_0/a$, where a is the radius of the electron beam, assumed round, at the interaction point.† Typically, b is of the order of some cm and a is of the order of 100 nm. If $\rho \gg 1$, only the photons with higher energy can meet at the i.p. and the spectrum becomes narrower. On the contrary, when $\rho \ll 1$ all kind of photons can collide and yield a broader luminosity spectrum.

Other effects on the luminosity distribution will be neglected such as multiple scattering of electrons in the laser, deflection by an external magnetic field (proposed to remove spent electrons from the interaction region [12]), synchrotron radiation between the conversion and the interaction point, etc. [13].

The cross section of the process $\gamma\gamma \to X$ with polarized photons can be written in the the Stokes-parameter and in the photon-helicity bases as

$$\mathrm{d}\hat{\sigma}_{\gamma\gamma} = \sum_{i,j=0}^{3} \xi_i \tilde{\xi}_j \mathrm{d}\hat{\sigma}_{ij} = \sum_{a,b,c,d=\pm} \rho_{ac}\tilde{\rho}_{bd} M_{ab} M^*_{cd} \mathrm{d}\Gamma, \tag{3}$$

where ξ_i, $\tilde{\xi}_j$ are the Stokes parameters of the first and second photon,‡ respectively; $\xi_0 = \tilde{\xi}_0 = 1$; $\rho_{\pm\pm} = \frac{1}{2}(1\pm\xi_2)$, $\rho_{+-} = \rho^*_{-+} = \frac{1}{2}(-\xi_3 + i\xi_1)$, and the same for $\tilde{\rho}$, are the photon polarization density matrices; M_{ab} are the invariant scattering amplitudes with photon helicities $a, b = \pm 1$; and $\mathrm{d}\Gamma$ is the corresponding element of phase space divided by the incoming flux.

Comparing both sides of Eq. (3), one finds sixteen independent real functions $\mathrm{d}\hat{\sigma}_{ij}$:

$$\frac{1}{4}\mathrm{d}\Gamma(|M_{++}|^2 + |M_{--}|^2 + |M_{+-}|^2 + |M_{-+}|^2) \quad = \quad \mathrm{d}\hat{\sigma}_{00} \equiv \mathrm{d}\hat{\sigma}$$

†Elliptical beams have been considered in [11].

‡Tilded parameters refer to the second photon.

$$
\begin{aligned}
\frac{1}{4}\mathrm{d}\Gamma(|M_{++}|^2+|M_{--}|^2-|M_{+-}|^2-|M_{-+}|^2) &= \mathrm{d}\hat{\sigma}_{22} \equiv \frac{1}{2}(\mathrm{d}\hat{\sigma}_0-\mathrm{d}\hat{\sigma}_2) \equiv \mathrm{d}\tau^a \\
\frac{1}{4}\mathrm{d}\Gamma(|M_{++}|^2-|M_{--}|^2+|M_{+-}|^2-|M_{-+}|^2) &= \mathrm{d}\hat{\sigma}_{20} \\
\frac{1}{4}\mathrm{d}\Gamma(|M_{++}|^2-|M_{--}|^2-|M_{+-}|^2+|M_{-+}|^2) &= \mathrm{d}\hat{\sigma}_{02} \\
\mathrm{d}\Gamma\mathsf{Re}(M_{++}M^*_{--}) &= \mathrm{d}\hat{\sigma}_{33}-\mathrm{d}\hat{\sigma}_{11} \equiv \mathrm{d}\hat{\sigma}_{||}-\mathrm{d}\hat{\sigma}_{\perp} \equiv \mathrm{d}\tau \\
\mathrm{d}\Gamma\mathsf{Im}(M_{++}M^*_{--}) &= (\mathrm{d}\hat{\sigma}_{13}+\mathrm{d}\hat{\sigma}_{31}) \\
\mathrm{d}\Gamma M_{+-}M^*_{-+} &= (\mathrm{d}\hat{\sigma}_{33}+\mathrm{d}\hat{\sigma}_{11})+i(\mathrm{d}\hat{\sigma}_{13}-\mathrm{d}\hat{\sigma}_{31}) \\
-\mathrm{d}\Gamma M_{++}M^*_{+-} &= (\mathrm{d}\hat{\sigma}_{03}+\mathrm{d}\hat{\sigma}_{23})+i(\mathrm{d}\hat{\sigma}_{01}+\mathrm{d}\hat{\sigma}_{21}) \\
-\mathrm{d}\Gamma M_{--}M^*_{-+} &= (\mathrm{d}\hat{\sigma}_{03}-\mathrm{d}\hat{\sigma}_{23})-i(\mathrm{d}\hat{\sigma}_{01}-\mathrm{d}\hat{\sigma}_{21}) \\
-\mathrm{d}\Gamma M_{++}M^*_{-+} &= (\mathrm{d}\hat{\sigma}_{30}+\mathrm{d}\hat{\sigma}_{32})+i(\mathrm{d}\hat{\sigma}_{10}+\mathrm{d}\hat{\sigma}_{12}) \\
-\mathrm{d}\Gamma M_{--}M^*_{+-} &= (\mathrm{d}\hat{\sigma}_{30}-\mathrm{d}\hat{\sigma}_{32})-i(\mathrm{d}\hat{\sigma}_{10}-\mathrm{d}\hat{\sigma}_{12}), \qquad (4)
\end{aligned}
$$

where $\mathrm{d}\hat{\sigma} = \frac{1}{2}(\mathrm{d}\hat{\sigma}_0+\mathrm{d}\hat{\sigma}_2) = \frac{1}{2}(\mathrm{d}\hat{\sigma}_{||}+\mathrm{d}\hat{\sigma}_{\perp})$ is the cross section for unpolarized photons, $\mathrm{d}\hat{\sigma}_0$ ($\mathrm{d}\hat{\sigma}_2$) are the cross sections for photons whose total helicity is 0 (± 2) and $\mathrm{d}\hat{\sigma}_{||}$ ($\mathrm{d}\hat{\sigma}_{\perp}$) for photons with parallel (orthogonal) linear polarizations.

Actually $M_{ab}M^*_{cd}$ is a shorthand notation for $M_{ab;r_i}M^*_{cd;r_i}$ where r_i labels the spin configuration of the particles in the final state X. In case that *Parity is conserved* in the process $\gamma\gamma \to X$,[§]

$$
M_{ab;r_i}M^*_{cd;r_i} = M_{-a-b;-r_i}M^*_{-c-d;-r_i} \qquad (5)
$$

and the final state polarizations are not analyzed, i.e. we perform a *sum over the final spins*, one has

$$
\begin{aligned}
|M_{++}|^2 &= |M_{--}|^2 \\
|M_{+-}|^2 &= |M_{-+}|^2 \\
M_{++}M^*_{--} &= M_{--}M^*_{++} \\
M_{+-}M^*_{-+} &= M_{-+}M^*_{+-} \\
M_{++}M^*_{+-} &= M_{--}M^*_{-+} \\
M_{--}M^*_{+-} &= M_{++}M^*_{-+}. \qquad (6)
\end{aligned}
$$

We are then left with eight independent functions: $\mathrm{d}\hat{\sigma}$, $\mathrm{d}\hat{\tau}^a \equiv \frac{1}{2}(\mathrm{d}\hat{\sigma}_0-\mathrm{d}\hat{\sigma}_2)$, $\mathrm{d}\hat{\tau} \equiv \mathrm{d}\hat{\sigma}_{||}-\mathrm{d}\hat{\sigma}_{\perp}$ and five more that drop if *azimuthal emission angles are integrated* [10]. Under all these assumptions, Eq. (3) is simplified to

$$
\mathrm{d}\hat{\sigma}_{\gamma\gamma} = \mathrm{d}\hat{\sigma} + \xi_2\tilde{\xi}_2\mathrm{d}\hat{\tau}^a + \frac{1}{2}(\xi_3\tilde{\xi}_3-\xi_1\tilde{\xi}_1)\mathrm{d}\hat{\tau}. \qquad (7)
$$

[§]Parity is not conserved in Higgs-boson production and this simplification will not be applied in that case. We will employ the simplified expressions only for the quark-pair production, which is a pure QED process at tree level.

Taking the colliding Compton-backscattered photons as the initial state for the process $\gamma\gamma \to X$, the event rate can be written as

$$\mathrm{d}N \equiv \mathrm{d}L \ \langle \mathrm{d}\hat{\sigma}_{\gamma\gamma} \rangle = \mathrm{d}L \sum_{i,j=0}^{3} \langle \xi_i \tilde{\xi}_j \rangle \mathrm{d}\hat{\sigma}_{ij}, \tag{8}$$

where $\mathrm{d}L$ is the differential $\gamma\gamma$ *luminosity* and $\langle \xi_i \tilde{\xi}_j \rangle$ is the average of the product of the Stokes parameters along the interaction region. Only the diagonal products of Stokes parameters are relevant as may be seen from (7).

3 The $\gamma\gamma$ luminosity

Let $\mathbf{P}_{\boldsymbol{c}}$ ($\mathbf{P}_{\boldsymbol{t}}$) be the mean circular (linear) laser polarization and $\boldsymbol{\zeta}_{||} = 2\boldsymbol{\lambda}_{\boldsymbol{e}}$ ($\boldsymbol{\zeta}_{\perp}$) the mean longitudinal (transverse) polarization of the electron/positron beam. Of course, ${\mathbf{P}_{\boldsymbol{c}}}^2 + {\mathbf{P}_{\boldsymbol{t}}}^2 \leq 1$, $(2\boldsymbol{\lambda}_{\boldsymbol{e}})^2 + {\boldsymbol{\zeta}_{\perp}}^2 \leq 1$, and the same for the polarizations of the second electron and laser beams. In the Gaussian beam approximation [10], the $\gamma\gamma$ luminosity reads

$$\mathrm{d}L = L_{\text{eff}} f_C(y) f_C(\tilde{y}) I_0(v) \exp\left\{ -\frac{\rho^2}{2} \left(\frac{y_m}{y} + \frac{y_m}{\tilde{y}} - 2 \right) \right\} M \delta(y\tilde{y} - z^2) \mathrm{d}y \mathrm{d}\tilde{y}, \tag{9}$$

where $z^2 \equiv W^2/s_{e^+e^-}$, W^2 is the two-photon invariant mass, $v \equiv \rho^2 \sqrt{(y_{\max}/y - 1)\,(y_{\max}/\tilde{y} - 1)}$ and $M \equiv 1 + A_1 \langle \cos\Psi \rangle + A_2 \langle \cos 2\Psi \rangle$, with $A_n(y, \tilde{y})$ being functions proportional to $\mathbf{P}_{\boldsymbol{t}} \tilde{\mathbf{P}}_{\boldsymbol{t}}$ [10]. The averages of azimuthal angles are given by $\langle \cos n\Psi \rangle = I_n(v)/I_0(v)$ where I_n are the modified Bessel functions of $n-$th order. For zero conversion distance $I_0(0) = 1$ and $I_{n>0}(0) = 0$. The total effective luminosity is $L_{\text{eff}} = k^2 L_{e^+e^-}$ where k^2 is a conversion coefficient.¶

In the Gaussian beam approximation the average of the Stokes-parameters $\langle \xi_i \tilde{\xi}_j \rangle$ can be obtained analytically as well [10]. We employ here an average at a fixed invariant mass,

$$\langle \xi_i \tilde{\xi}_j \rangle_z \equiv \int_y \ \mathrm{d}L \ \langle \xi_i \tilde{\xi}_j \rangle \Big/ \int_y \mathrm{d}L \ , \tag{10}$$

which is of interest since the $\gamma\gamma \to X$ cross section does not depend on the rapidity of the two-photon system (equivalently the energy fraction y of one of the laser photons).

To illustrate some polarization effects that will be exploited later, we consider below two different polarizations for the lasers, assuming arbitrary longitudinal polarizations $\boldsymbol{\lambda}_{\boldsymbol{e}}$, $\tilde{\boldsymbol{\lambda}}_{\boldsymbol{e}}$ for the electron/positron beams.

¶Alhough $L_{\text{eff}} < L_{e^+e^-}$, the $\gamma\gamma$ luminosity can be larger than the e^+e^- luminosity because of the absence of beam-beam effects that allows a larger $L_{e^+e^-}$ [12]. On the other hand, for $\rho \geq 0$, $\int \mathrm{d}L \leq L_{\text{eff}}$ which produces an additional reduction in the total luminosity available.

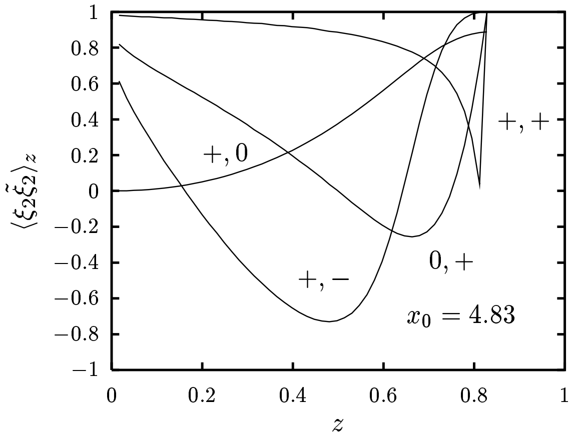

Figure 1: The average $\langle\xi_2\tilde{\xi}_2\rangle_z$ for $x_0 = 4.83$ and several values of the electron longitudinal and laser circular polarizations $(\boldsymbol{\lambda_e}, \mathbf{P_c})$, taking the same configuration for both arms of the collider: $\boldsymbol{\lambda_e} = \tilde{\boldsymbol{\lambda}}_{\boldsymbol{e}}$ and $\mathbf{P_c} = \tilde{\mathbf{P}}_{\boldsymbol{c}}$. For the case $\boldsymbol{\lambda_e} = -\tilde{\boldsymbol{\lambda}}_{\boldsymbol{e}}$ and $\mathbf{P_c} = -\tilde{\mathbf{P}}_{\boldsymbol{c}}$ all the curves change sign.

3.1 Circularly polarized lasers

The relevant averages of Stokes parameters yield

$$\begin{aligned} \langle\xi_2\tilde{\xi}_2\rangle &= \langle\xi_2\rangle\langle\tilde{\xi}_2\rangle = \xi_2\tilde{\xi}_2, \\ \langle\xi_3\tilde{\xi}_3\rangle &= -\langle\xi_1\tilde{\xi}_1\rangle \equiv \Lambda. \end{aligned} \tag{11}$$

Λ vanishes for $\rho = 0$ and has very small values otherwise, in particular when $y \sim \tilde{y} \sim y_{\rm max}$.

The average $\langle\xi_2\tilde{\xi}_2\rangle_z$ (Fig. 1) is, on the contrary, independent of conversion distance effects for circularly polarized photons. The event rate (8) can be very conveniently rewritten as

$$\begin{aligned} \mathrm{d}N &= \mathrm{d}L^{J_z=0}\ \mathrm{d}\hat{\sigma}_0 + \mathrm{d}L^{J_z=\pm 2}\ \mathrm{d}\hat{\sigma}_2, \\ \mathrm{d}L^{J_z=0} &\equiv \frac{1}{2}\mathrm{d}L\ (1+\langle\xi_2\tilde{\xi}_2\rangle), \quad \mathrm{d}L^{J_z=\pm 2} \equiv \frac{1}{2}\mathrm{d}L\ (1-\langle\xi_2\tilde{\xi}_2\rangle), \end{aligned} \tag{12}$$

where a contribution $\mathrm{d}L\ \langle\xi_3\tilde{\xi}_3 - \xi_1\tilde{\xi}_1\rangle$ has been safely neglected.

3.2 Linearly polarized lasers

Neglecting $\rho \neq 0$ effects, fully accounted for in our numerical calculations, one can write

$$\begin{aligned} \langle\xi_2\tilde{\xi}_2\rangle &\simeq \langle\xi_2\rangle\langle\tilde{\xi}_2\rangle = 4\boldsymbol{\lambda_e}\tilde{\boldsymbol{\lambda}}_{\boldsymbol{e}}\ \mathcal{C}\tilde{\mathcal{C}} \\ \langle\xi_3\tilde{\xi}_3 - \xi_1\tilde{\xi}_1\rangle &\simeq \langle\xi_3\rangle\langle\tilde{\xi}_3\rangle - \langle\xi_1\rangle\langle\tilde{\xi}_1\rangle = \mathbf{P_t}\tilde{\mathbf{P}}_{\boldsymbol{t}}\ \ell\tilde{\ell}\cos 2(\Delta\gamma). \end{aligned} \tag{13}$$

$\Delta\gamma$ is the angle between the planes of maximal linear polarization of both lasers.

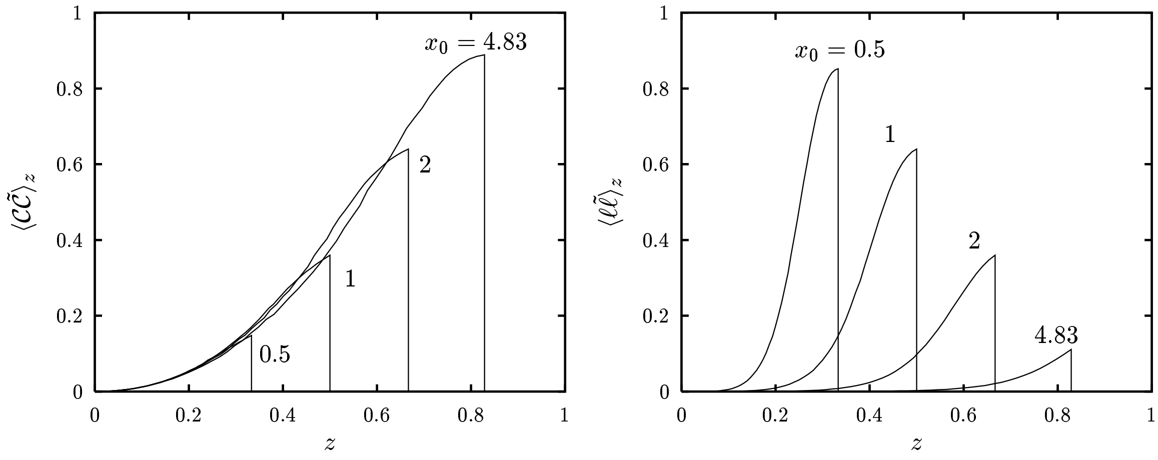

Figure 2: The correlations $\langle \mathcal{C}\tilde{\mathcal{C}}\rangle_z$ and $\langle \ell\tilde{\ell}\rangle_z$, relevant for linearly polarized laser beams (13), for different values of x_0.

Both the induced circular $\mathcal{C}$ and linear ℓ polarizations of the backscattered photons are growing functions with y (Fig. 2). But, while the circular polarization is larger for high values of x_0, the longitudinal one is enhanced for low values of x_0. For this configuration it results more convenient to cast (8) into

$$\begin{aligned} \mathrm{d}N &= \mathrm{d}L^{||}\ \mathrm{d}\hat{\sigma}_{||} + \mathrm{d}L^{\perp}\ \mathrm{d}\hat{\sigma}_{\perp} + \mathrm{d}L^{C}\ \mathrm{d}\hat{\tau}^{a}, \\ \mathrm{d}L^{||} &\equiv \frac{1}{2}\mathrm{d}L\ (1 + \langle \xi_3\tilde{\xi}_3 - \xi_1\tilde{\xi}_1\rangle),\ \mathrm{d}L^{\perp} \equiv \frac{1}{2}\mathrm{d}L\ (1 - \langle \xi_3\tilde{\xi}_3 - \xi_1\tilde{\xi}_1\rangle),\ \mathrm{d}L^{C} \equiv \mathrm{d}L\ \langle \xi_2\tilde{\xi}_2\rangle. \quad (14) \end{aligned}$$

The contribution $\mathrm{d}L^C$ is roughly proportional to the product of the longitudinal polarizations of electron/positron beams (13) and plays an important role for background suppression: since the $q\bar{q}$ background far from threshold has mostly $J_z = \pm 2$, the term $\mathrm{d}\tau^a$ is negative and the contribution proportional to $\mathrm{d}L^C$ further suppresses the background by choosing like-handed polarized linac beams ($\boldsymbol{\lambda_e}\tilde{\boldsymbol{\lambda}}_{\boldsymbol{e}} > 0$).

3.3 Luminosity spectrum

The resulting luminosity spectrum for the various components and different polarizations is displayed in Fig. 3. We assume realistic degrees of longitudinal electron polarization (85%) and laser polarizations (both circular and linear close to 100% seem feasible [14]).

For circularly polarized lasers [8] (Fig. 3a), a *broad* spectrum (dashed lines) can be achieved by employing electrons and laser photons with like-handed helicities (see (+,+) in Fig. 1) and a small value of $\rho = 0.6$ to allow low energetic backscattered photons in the interaction region. On the contrary, a *sharp* spectrum (solid lines) peaking in the vicinity of $z = y_{\max}$ can be obtained using opposite-handed electrons and laser photons (see (+,−) in Fig. 1) in a more

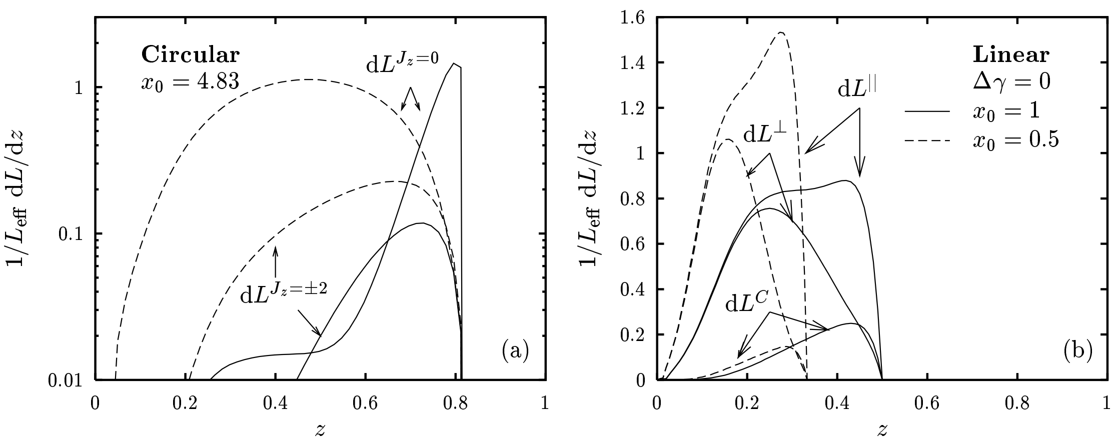

Figure 3: Normalized luminosities for circularly polarized lasers (a); and linearly polarized lasers with $\Delta\gamma = 0$ (b). The lasers are assumed to be completely polarized and the electrons 85% longitudinally polarized. Identical configurations are taken for both arms of the collider. In (a) $x_0 = 4.83$ and solid (dashed) lines are for opposite-handed (like-handed) photons and electrons with $\rho = 3.0$ ($\rho = 0.6$). In (b) $\rho = 0.6$, $\boldsymbol{\lambda_e} = \boldsymbol{\tilde{\lambda}_e} = 0.85/2$ and $x_0 = 1$ ($x_0 = 0.5$) for solid (dashed) lines.

restrictive interaction region $\rho = 3.0$. The $J_z = 0$ events (containing maybe the Higgs signal) are efficiently enhanced and the $J_z = \pm 2$ components (including the non-Higgs background) are suppressed by tuning lasers and linac beams so that $x_0 = 4.83$ (maximal profit of the collider energy). The peak takes place at $z_{\rm opt} \approx 0.8$. One can obtain Higgs bosons with $M_\varphi \lesssim 400$ (800) GeV at a linac energy $\sqrt{s_{e^+e^-}} = 500$ GeV (1 TeV).

For linearly polarized lasers, a small $\rho = 0.6$ has been chosen. The case of parallel laser polarizations ($\Delta\gamma = 0$) is shown in Fig. 3b. For $\Delta\gamma = \pi/2$ the roles of $\mathrm{d}L^{||}$ and $\mathrm{d}L^{\perp}$ get exchanged. There is a compromise between getting a good separation of the $||$ and $\perp$ components (small x_0 is preferred) and producing a heavy enough Higgs boson, since the energy available is proportional to $x_0/(x_0+1)$. The best solution consists of choosing the minimum possible value of x_0 and tuning the linac and laser energies to

$$\sqrt{s_{e^+e^-}} \quad = \quad \frac{M_\varphi}{z_{\rm opt}} \tag{15}$$

$$\omega_0 \quad = \quad \frac{m_e^2}{2M_\varphi} x_0 z_{\rm opt} \simeq 130\ x_0 z_{\rm opt}\ \frac{\rm eV}{M_\varphi/\rm GeV} \tag{16}$$

so that the Higgs boson sits on an optimal

$$z_{\rm opt} = \alpha(x_0)\frac{x_0}{x_0+1} \tag{17}$$

with $\alpha(x_0) \simeq 0.9$ for $x_0 \lesssim 1$ [15]. Such tunable linac and laser energies, $\sqrt{s_{e^+e^-}} \lesssim 1$ TeV and $\omega_0 \sim 0.1 \div 1$ eV, are foreseen [16]. In this operation mode, assuming a maximal linac energy

$\sqrt{s_{e^+e^-}} = 500$ GeV (1 TeV), one can produce Higgs bosons with masses up to $M_\varphi = 150$ (300) GeV for $x_0 = 0.5$, and $M_\varphi = 225$ (450) GeV for $x_0 = 1.0$. Of course larger values of x_0 could be tuned to produce heavier Higgs bosons but then the distinction of their CP-parity becomes more difficult.

4 Higgs-boson phenomenology at the PLC

4.1 Resonant production of Higgs bosons

The production of a spin-0 CP-eigenstate φ by the fusion of two photons, $\gamma\gamma \to \varphi$, proceeds via $F_{\mu\nu}F^{\mu\nu}\varphi$ for a scalar field, and $F_{\mu\nu}\tilde{F}^{\mu\nu}\varphi$ for a pseudoscalar. The corresponding Feynman rules for such couplings are proportional to $\epsilon \cdot \tilde{\epsilon}$ and $(\epsilon \times \tilde{\epsilon})_z$, respectively, for two back-to-back photons moving along the z-axis. The amplitude for a general spin-0 state coupled to two photons can be written as

$$M_{\lambda\tilde{\lambda}} = (\epsilon \cdot \tilde{\epsilon})\ \mathcal{E} + (\epsilon \times \tilde{\epsilon})_z\ \mathcal{O}, \tag{18}$$

where $\mathcal{E}$ ($\mathcal{O}$) are the CP-even(odd) contributions to the amplitude. CP is violated if *both* terms are not vanishing. In any case the coupling for opposite helicity photons vanishes ($M_{+-} = M_{-+} = 0$). There are four independent functions describing the process, out of the sixteen in (4),

$$\begin{aligned}
\mathrm{d}\hat{\sigma}_{00} + \mathrm{d}\hat{\sigma}_{22} &= \frac{1}{2}\mathrm{d}\Gamma(|M_{++}|^2 + |M_{--}|^2) = |\mathcal{E}|^2 + |\mathcal{O}|^2 \\
\mathrm{d}\hat{\sigma}_{20} + \mathrm{d}\hat{\sigma}_{02} &= \frac{1}{2}\mathrm{d}\Gamma(|M_{++}|^2 - |M_{--}|^2) = -2\mathsf{Im}(\mathcal{E}\mathcal{O}^*) \\
\mathrm{d}\hat{\sigma}_{31} + \mathrm{d}\hat{\sigma}_{13} &= \mathrm{d}\Gamma\mathsf{Im}(M_{++}M_{--}^*) = -2\mathsf{Re}(\mathcal{E}\mathcal{O}^*) \\
\mathrm{d}\hat{\sigma}_{33} - \mathrm{d}\hat{\sigma}_{11} &= \mathrm{d}\Gamma\mathsf{Re}(M_{++}M_{--}^*) = |\mathcal{E}|^2 - |\mathcal{O}|^2.
\end{aligned} \tag{19}$$

Defining the asymmetries [17]:

$$\begin{aligned}
\mathcal{A}_1 &\equiv \frac{|M_{++}|^2 - |M_{--}|^2}{|M_{++}|^2 + |M_{--}|^2} = -\frac{2\mathsf{Im}(\mathcal{E}\mathcal{O}^*)}{|\mathcal{E}|^2 + |\mathcal{O}|^2} \\
\mathcal{A}_2 &\equiv \frac{2\mathsf{Im}(M_{++}M_{--}^*)}{|M_{++}|^2 + |M_{--}|^2} = -\frac{2\mathsf{Re}(\mathcal{E}\mathcal{O}^*)}{|\mathcal{E}|^2 + |\mathcal{O}|^2} \\
\mathcal{A}_3 &\equiv \frac{2\mathsf{Re}(M_{++}M_{--}^*)}{|M_{++}|^2 + |M_{--}|^2} = \frac{|\mathcal{E}|^2 - |\mathcal{O}|^2}{|\mathcal{E}|^2 + |\mathcal{O}|^2},
\end{aligned} \tag{20}$$

the event rate (8) is

$$\begin{aligned}
\mathrm{d}N &= \mathrm{d}L^{S=0}\ \mathrm{d}\hat{\sigma}, \\
\mathrm{d}L^{S=0} &\equiv \mathrm{d}L\ [\ 1 + \langle\xi_2\tilde{\xi}_2\rangle + \langle\xi_2 + \tilde{\xi}_2\rangle\ \mathcal{A}_1 + \langle\xi_3\tilde{\xi}_1 + \xi_1\tilde{\xi}_3\rangle\ \mathcal{A}_2 + \langle\xi_3\tilde{\xi}_3 - \xi_1\tilde{\xi}_1\rangle\ \mathcal{A}_3\ ],
\end{aligned} \tag{21}$$

with the unpolarized $\gamma\gamma \to \varphi$ cross section being $\mathrm{d}\hat{\sigma} = \frac{1}{4}\mathrm{d}\Gamma(|M_{++}|^2 + |M_{--}|^2)$. Recalling the remarks above (7), expression (21) shows that one has to analyze the spins and/or the azimuthal emission angles of the final state to probe CP violation through the asymmetries $\mathcal{A}_1$ and $\mathcal{A}_2$.

For φ being a CP-eigenstate with $\eta^{\varphi}_{\rm CP} = \pm 1$ for $\varphi = H, A$ (scalar or pseudoscalar, respectively), one has $\mathcal{A}_1 = \mathcal{A}_2 = 0$, $\mathcal{A}_3 = \eta^{\varphi}_{\rm CP}$ and (21) simplifies to

$$\mathrm{d}L^{S=0} = \mathrm{d}L^{0^{\eta^{\varphi}_{\rm CP}}} \equiv \mathrm{d}L \; [\; 1 + \langle \xi_2 \tilde{\xi}_2 \rangle + \eta^{\varphi}_{\rm CP} \langle \xi_3 \tilde{\xi}_3 - \xi_1 \tilde{\xi}_1 \rangle \;]. \tag{22}$$

In fact, if CP is conserved, $M_{++} = \eta^{\varphi}_{\rm CP} M_{--}$ and, since $\mathrm{d}\Gamma \mathsf{Re}(M_{++}M^*_{--}) = \mathrm{d}\hat{\sigma}_{||} - \mathrm{d}\hat{\sigma}_{\perp} = \eta^{\varphi}_{\rm CP} \cdot (\mathrm{d}\hat{\sigma}_{||} + \mathrm{d}\hat{\sigma}_{\perp})$, only photons with parallel (orthogonal) linear polarizations couple to scalars (pseudoscalars), in agreement with (18). We concentrate on this case (CP conservation) in our analysis. It corresponds to the MSSM with real parameters.[‖] Notice that *only if the lasers are linearly polarized* it is then possible to distinguish the CP nature of the Higgs field, since the average $\langle \xi_3 \tilde{\xi}_3 - \xi_1 \tilde{\xi}_1 \rangle$ is negligible for circularly polarized lasers (11).

4.2 The H and A decays

The Higgs spectrum of the MSSM is determined at tree level by two independent parameters, the pseudoscalar mass M_A and the ratio of the two vacuum expectation values $\tan\beta$. For the evaluation of the Higgs boson decays we have employed an adapted version of the program `HDECAY` [19]. We have explored two scenarios, low and high $\tan\beta$ ($\tan\beta = 2, 50$, respectively) and taken a reference set of MSSM input parameters for which the decays of the neutral Higgs bosons into supersymmetric particles are kinematically suppressed or forbidden in the studied range of Higgs boson masses: $\mu = -250$ GeV, $M_2 = m_{\tilde{Q}} = 1$ TeV and both no-mixing and maximal mixing in the squark sector, $A_t = 0$ and $A_t = \sqrt{6} m_{\tilde{Q}}$, respectively. We present here only the case of no-mixing. The squark mixing does not play a relevant role for the heavy Higgs sector. GUT gaugino-mass constraints and universal supersymmetric soft-breaking terms are assumed. The main decay channels of H and A are the following [20]. In the low $\tan\beta$ region, one must distinguish two Higgs mass ranges: below the top-pair threshold, H decays most often to light Higgs-pairs hh (or to WW^* for $M_H \lesssim 200$ GeV if there is maximal mixing) and A goes to $b\bar{b}$ ($M_A \lesssim 200$ GeV) and hZ (otherwise); whereas H and A decay fully to $t\bar{t}$ for $M_\varphi \gtrsim 2m_t$. If $\tan\beta$ is large, both H and A decay almost fully into $b\bar{b}$ pairs.

The background to these Higgs signals comes mainly from the continuum (non-Higgs) production of the same final states. The processes $\gamma\gamma \to hh$ [21] and $\gamma\gamma \to Zh$ are considered as negligible backgrounds [15].

‖Actually, some of the parameters of the MSSM can be complex. In this case, physical phases may be introduced that produce CP-violating effects, through the one-loop coupling of the Higgs field to two photons. A detailed study of the photon collider capabilities to probe CP violation in the MSSM Higgs sector of the MSSM has been recently presented in [18].

4.3 Effective cross sections

Since the process under study proceeds through a narrow resonance, one must take into account the detector accuracy when comparing signal (resonant production) and background (continuum production). An appropriate way to obtain *effective* signal and background consists of integrating a window of two-photon invariant masses $(M_\varphi - \Delta, M_\varphi + \Delta)$ around the Higgs mass assuming the reconstruction resolution is a Gaussian [8]. That is, making use of (8),

$$\begin{aligned} N_{\text{eff}}(M_\varphi) &\equiv L_{\text{eff}} \mathrm{d}\sigma_{\text{eff}} \equiv \int_{M_\varphi-\Delta}^{M_\varphi+\Delta} \mathrm{d}N_{\text{eff}}(W), \\ \mathrm{d}N_{\text{eff}}(W) &\equiv \int_{M_X}^{y_{\max}\sqrt{s_{e^+e^-}}} \frac{\mathrm{d}W'}{\sqrt{2\pi}\delta} \exp\left\{-\frac{(W'-W)^2}{2\delta^2}\right\} \frac{\mathrm{d}L}{\mathrm{d}W'} \langle \mathrm{d}\hat{\sigma}_{\gamma\gamma} \rangle. \end{aligned} \tag{23}$$

The signal cross section $\gamma\gamma \to \varphi \to X$ for polarized photons, $\hat{\sigma}_{\gamma\gamma}^{\text{signal}}$, is *isotropic* and can be written as

$$\hat{\sigma}_{\gamma\gamma}^{\text{signal}}(W) = 8\pi \frac{\Gamma(\varphi \to \gamma\gamma)\Gamma(\varphi \to X)}{(W^2 - M_\varphi^2)^2 + \Gamma_\varphi^2 M_\varphi^2}(1 + \lambda\tilde{\lambda}). \tag{24}$$

For the regions where the width is much smaller than the detector resolution the following relation can be used**

$$N_{\text{eff}}^{\text{signal}}(M_\varphi) \simeq R(\Delta/\delta) \left.\frac{\mathrm{d}L^{S=0}}{\mathrm{d}W}\right|_{W=M_\varphi} \times 4\pi^2 \frac{\Gamma(\varphi \to \gamma\gamma)\mathrm{BR}(\varphi \to X)}{M_\varphi^2}, \tag{25}$$

where the Gaussian error function describing the fraction of signal events contained in the bin $M_\varphi \pm \Delta$ is $R(\Delta/\delta) = 0.9545$ for $\Delta = 2\delta$ (standard deviations) and $\mathrm{d}L^{S=0}$ is the $\gamma\gamma$ luminosity for the production of a spin-0 state (21). Assuming a resolution of $\delta = 2.5$ GeV, it is safe to use approximation (25) only for an intermediate Higgs boson mass (standard or supersymmetric) but it overestimates the production rates for heavier Higgs bosons. The MSSM Higgs widths can be $\Gamma_\varphi \approx 5$ GeV for $M_\varphi \lesssim 500$ GeV (and much larger for the SM Higgs boson) though $\Gamma_\varphi \lesssim 0.1$ GeV for masses below the top-pair threshold [20].

The effective background $\gamma\gamma \to X$ for an invariant mass $W = M_\varphi$ is approximated by

$$N_{\text{eff}}^{\text{bckg}}(W) \simeq 2\Delta \frac{\mathrm{d}L}{\mathrm{d}W} \langle \mathrm{d}\hat{\sigma}_{\gamma\gamma}^{\text{bckg}}(W) \rangle, \tag{26}$$

assuming the distribution of invariant masses weighted with the luminosity spectrum is smooth enough. The main source of continuum background to the Higgs boson production is the quark-pair production. The total Born cross sections $\gamma\gamma \to q\bar{q}$ ($\hat{\sigma}_0$, $\hat{\sigma}_2$ and $\hat{\tau} \equiv \hat{\sigma}_{||} - \hat{\sigma}_\perp$) for a polar cut in the two-photon center of mass system $|\cos\vartheta^*| < c$ are

$$\hat{\sigma}_0(W) = \frac{12\pi\alpha^2 Q_q^4}{W^2}(1-\beta^4)\left\{\frac{1}{2}\ln\frac{1+c\beta}{1-c\beta} + \frac{c\beta}{1-(c\beta)^2}\right\} \tag{27}$$

**The Breit-Wigner distribution $\dfrac{1}{\pi}\dfrac{\Gamma M}{(W^2-M^2)+\Gamma^2 M^2} \simeq \delta(W^2 - M^2) = \dfrac{1}{2M}\delta(W-M)$ for $\Gamma \ll M$.

$$\hat{\sigma}_2(W) = \frac{12\pi\alpha^2 Q_q^4}{W^2}\left\{\frac{5-\beta^4}{2}\ln\frac{1+c\beta}{1-c\beta} - c\beta\left[2+\frac{(1-\beta^2)(3-\beta^2)}{1-(c\beta)^2}\right]\right\} \tag{28}$$

$$\hat{\tau}(W) = \hat{\sigma}_{||} - \hat{\sigma}_{\perp} = \frac{12\pi\alpha^2 Q_q^4}{W^2}(1-\beta^2)^2\left\{\frac{1}{2}\ln\frac{1+c\beta}{1-c\beta} + \frac{c\beta}{1-(c\beta)^2}\right\} < 0 \tag{29}$$

with $\beta = \sqrt{1-4m_q^2/W^2}$ and Q_q the electric charge of the quark q. We take the usual $c = 0.7$ that helps to eliminate a great deal of background events in comparison to only a 30% reduction of signal events. In practice this means a cut on the difference of rapidities of both jets/tops given by $|\Delta\eta| \leq |\ln[(1+\beta c)/(1-\beta c)]|$.

The background cross sections receive important QCD radiative corrections [22], particularly large for the $J_z = 0$ component, and also significant electroweak corrections [23]. The QCD corrections to the interference term (29) are not yet available [24]. In this preliminary analysis we ignore them all: the statistical significances of the Higgs signals should not change dramatically and the CP asymetries will not suffer a large distortion due to the background as long as $\hat{\sigma}_{||}$ and $\hat{\sigma}_{\perp}$ are corrected by similar amounts. However, all relevant QCD and electroweak corrections to the Higgs production and decay are incorporated in `HDECAY` [19, 20].

There is of course no interference between the H and A amplitudes, owing to their opposite CP-parity, even if their masses are very close, as it is usually the case, since we consider *unpolarized* final states. We neglect the interference between the resonant production and the continuum background, although it may be relevant because of the not so narrow width of the Higgs bosons, particularly for very high masses.[††]

In Fig. 4 we show the cross sections (before folding with the $\gamma\gamma$ luminosity) for $\gamma\gamma \to X$ and $\gamma\gamma \to H/A \to X$. The resonant ones are normalized assuming the events collected in an interval of invariant masses around $W = M_\varphi$ with a width $2\Delta = 10$ GeV. The $q\bar{q}$ events in the continuum and far from threshold ($b\bar{b}$ and $c\bar{c}$ pairs) are mainly in the $J_z = \pm 2$ state. They are produced by photons with perpendicular and parallel polarizations at the same rate. Near threshold ($t\bar{t}$ pairs) the $J_z = 0$ component dominates and the quark-pairs couple mostly to perpendicularly polarized photons.

5 The case of circularly polarized lasers

Circularly polarized lasers can produce the largest luminosities (Fig. 3a) for the Higgs signal (22) and, at the same time, the $J_z = 0$ component of the continuum background (12). The latter is suppressed far from the $q\bar{q}$ threshold (Fig. 4). The broad spectrum in Fig. 3a (dashed lines) for a fixed collider energy is clearly optimal for discovery; the sharp one (solid lines),

[††]See Ref. [25] for a very recent analysis of the interferences between H and A with small mass gap and between them and the continuum for polarized top-pairs in the final state. There it is proposed an alternative method to measure the CP-parity of the Higgs bosons based on these interferences. It appears not so efficient as the one analyzed here.

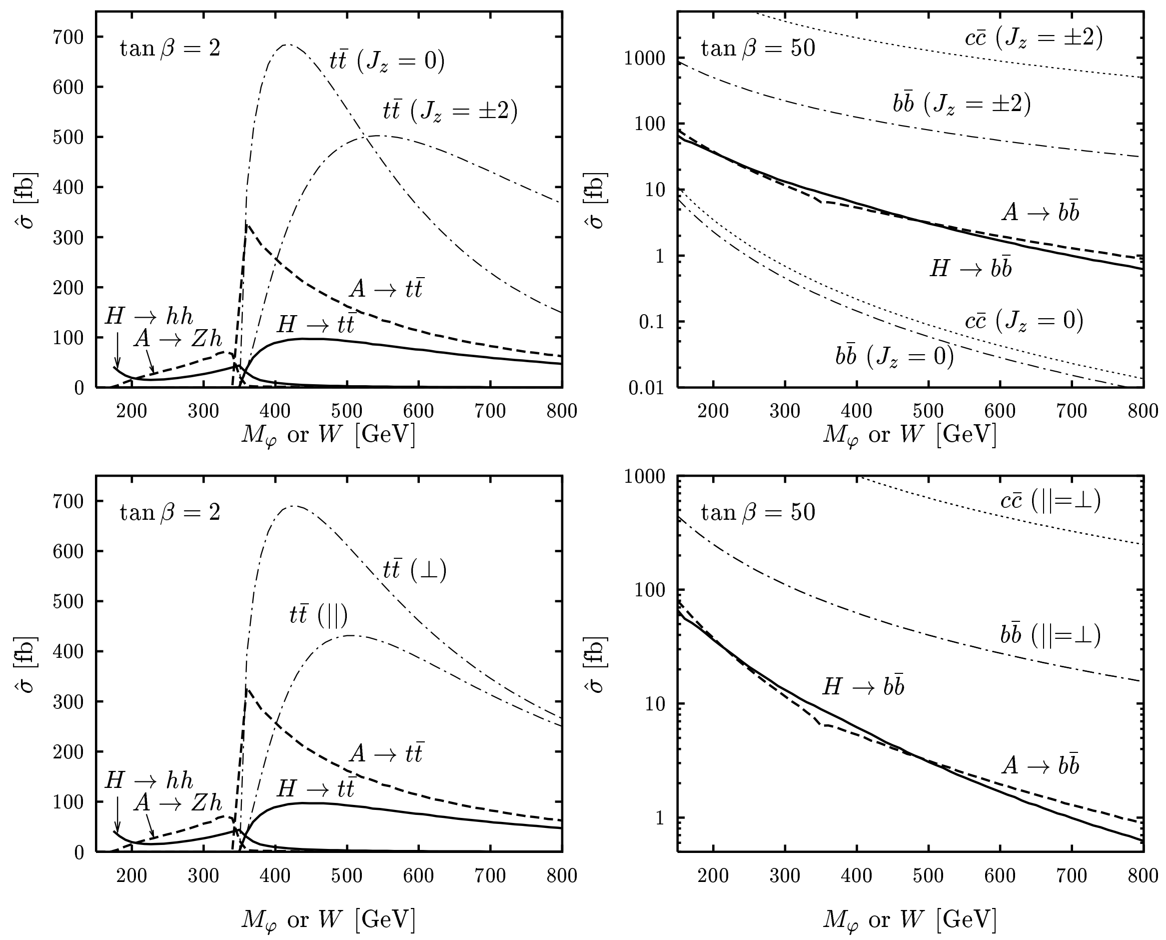

Figure 4: The Born cross sections ($|\cos\vartheta^*| < 0.7$) for relevant signals and backgrounds, before folding with the $\gamma\gamma$ luminosity, for two scenarios of $\tan\beta$. They are split into initial states of $J_z = 0$ and $J_z = \pm 2$ (above), and parallel ($||$) and perpendicular ($\perp$) photon linear polarizations (below). They are normalized as explained in the text.

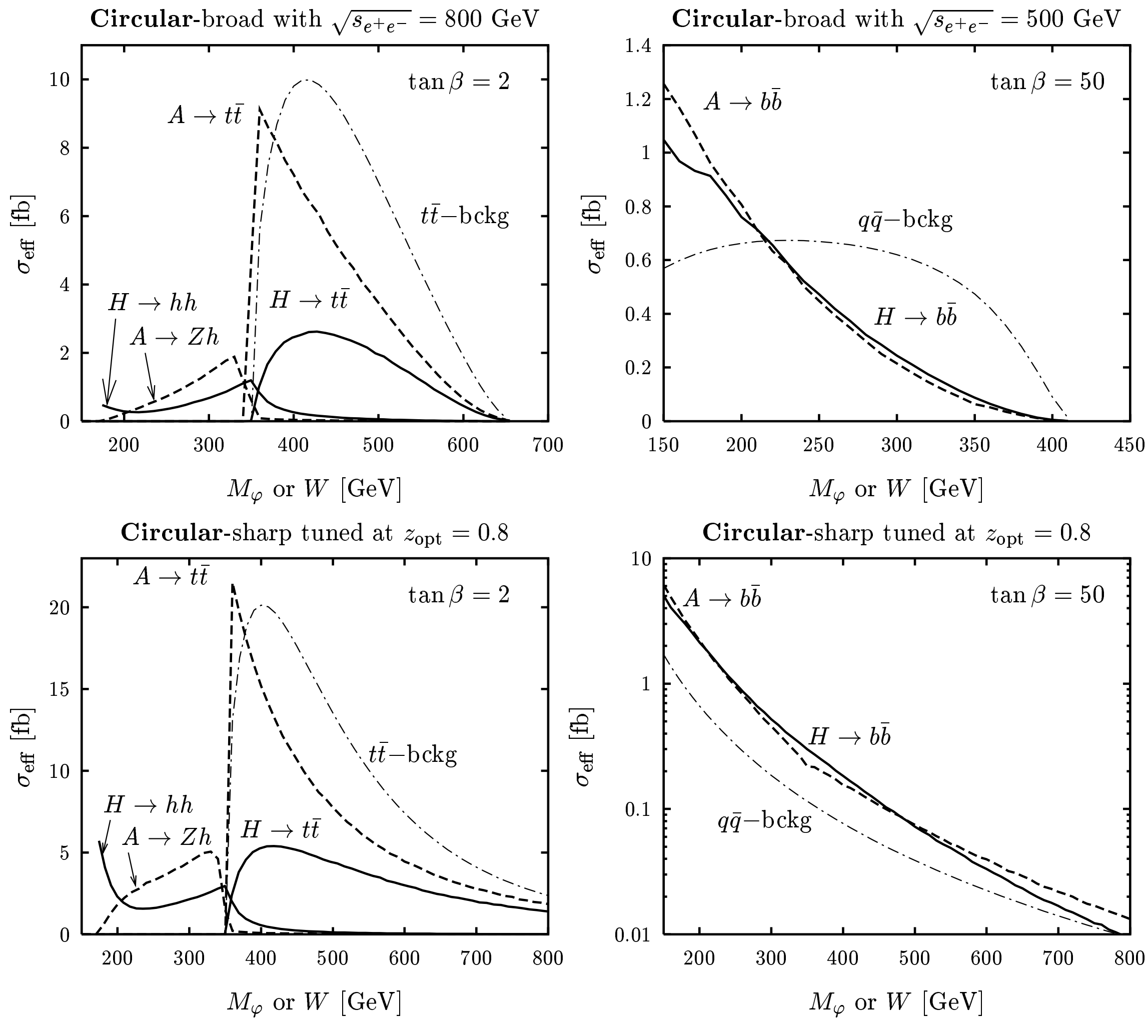

Figure 5: The effective cross sections for the H and A signals and their backgrounds in two $\tan\beta$ scenarios and for two modes of operation of the PLC, both with circular laser polarizations. 50% $b\bar{b}$-tagging efficiency and 5% $c\bar{c}/b\bar{b}$ contamination have been assumed.

for a collider energy tuned at the peak, is the best to reduce the large $J_z = \pm 2$ component of the background. The same is true for an intermediate Higgs mass [8]. The determination of the CP-parity of the Higgs field is not possible using circularly polarized lasers, as already mentioned.

These expectations are illustrated in Fig. 5, where the $\gamma\gamma$ luminosities of Fig. 3a have been assumed. For the $b\bar{b}$ channel we have considered a 50% $b\bar{b}$-tagging efficiency and the possibility of a 5% $c\bar{c}/b\bar{b}$ contamination. The $t\bar{t}$ pairs are supposed to be fully identified. The hh and Zh channels are taken free of background.

For low $\tan\beta$ the A signal dominates over H, but in the large $\tan\beta$ region both H and A are produced with similar rates. This is because the production rates are roughly proportional to the two-photon decay width of the corresponding Higgs boson (24,25), which is much larger for the pseudoscalar if $\tan\beta$ is small [27]. On the other hand the production rates are smaller for high $\tan\beta$, in particular for large Higgs masses, due to the smaller two-photon widths when $\tan\beta$ is large and to the smearing of the resosonance (the total Higgs-boson widths grow with $\tan\beta$).

For the $t\bar{t}$ channel the background is large because near threshold the pairs produced in the continuum have a large $J_z = 0$ component. Conversely, the background suppression is very effective in the $b\bar{b}$ channel, especially for the sharp spectrum running in the tuned-energy mode.

In the fixed-energy mode, we have taken $\sqrt{s_{e^+e^-}} = 800$ GeV in order to better explore the low $\tan\beta$ region, dominated by the $t\bar{t}$ channel above threshold, and $\sqrt{s_{e^+e^-}} = 500$ GeV for the high $\tan\beta$ scenario where the Higgs bosons decay into $b\bar{b}$ pairs. Larger statistics are obtained for the sharp spectrum in the tuned-energy mode ($\sqrt{s} = M_\varphi / z_{\rm opt}$).

The statistical significances for the Higgs signals, defined by

$$N_{SD}(\varphi) = \frac{\sigma^\varphi_{\rm eff}}{\sqrt{\sigma^\varphi_{\rm eff} + \sigma^{\rm bckg}_{\rm eff}}} \sqrt{L_{\rm eff}}, \tag{30}$$

are shown in Fig. 6, assuming $L_{\rm eff} = 100\ {\rm fb}^{-1}$. A range of both H and A Higgs masses up to the kinematical limit $M_\varphi \approx 0.8\sqrt{s_{e^+e^-}}$ can be covered with statistical significances of several standard deviations, particularly for not very large masses, in both $\tan\beta$ scenarios, even in the fixed-energy mode.

6 The case of linearly polarized lasers

Linearly polarized lasers (Fig. 3b) are necessary to distinguish the CP-parity of the Higgs bosons. The asymmetry $\mathcal{A}_3$ in (20) is probed by taking the difference of the event rates with $\Delta\gamma = 0$ (lasers with parallel polarizations) and with $\Delta\gamma = \pi/2$ (lasers with perpendicular polarizations) [15, 17, 26],

$$\langle \mathcal{A}^\varphi_3 \rangle = \frac{\sigma_{\rm eff}(\Delta\gamma = 0) - \sigma_{\rm eff}(\Delta\gamma = \pi/2)}{\sigma_{\rm eff}(\Delta\gamma = 0) + \sigma_{\rm eff}(\Delta\gamma = \pi/2)}, \tag{31}$$

where the contamination from a possible background is included in $\sigma_{\rm eff} \equiv \sigma^\varphi_{\rm eff} + \sigma^{\rm bckg}_{\rm eff}$. In terms of the linac and laser polarizations this asymmetry reads

$$\langle \mathcal{A}^\varphi_3 \rangle \simeq \mathbf{P}_t \tilde{\mathbf{P}}_t \langle \ell\tilde{\ell} \rangle_{z_{\rm opt}} \frac{\eta^\varphi_{\rm CP} \hat{\sigma}^\varphi + \frac{1}{2}(\hat{\sigma}^{\rm bckg}_{||} - \hat{\sigma}^{\rm bckg}_{\perp})}{\frac{1}{2}(1 + 4\boldsymbol{\lambda}_e \tilde{\boldsymbol{\lambda}}_e \langle \mathcal{C}\tilde{\mathcal{C}} \rangle_{z_{\rm opt}})(2\hat{\sigma}^\varphi + \hat{\sigma}^{\rm bckg}_0) + \frac{1}{2}(1 - 4\boldsymbol{\lambda}_e \tilde{\boldsymbol{\lambda}}_e \langle \mathcal{C}\tilde{\mathcal{C}} \rangle_{z_{\rm opt}}) \hat{\sigma}^{\rm bckg}_2}. \tag{32}$$

The $\rho \neq 0$ effects have been dropped in the previous equation but are included in the numerical calculations. This expression explains the importance of linear laser polarizations, $\mathbf{P}_t$, $\tilde{\mathbf{P}}_t$, the role of the linac longitudinal polarizations, $\boldsymbol{\lambda}_e$, $\tilde{\boldsymbol{\lambda}}_e$, and the effect of the different components of

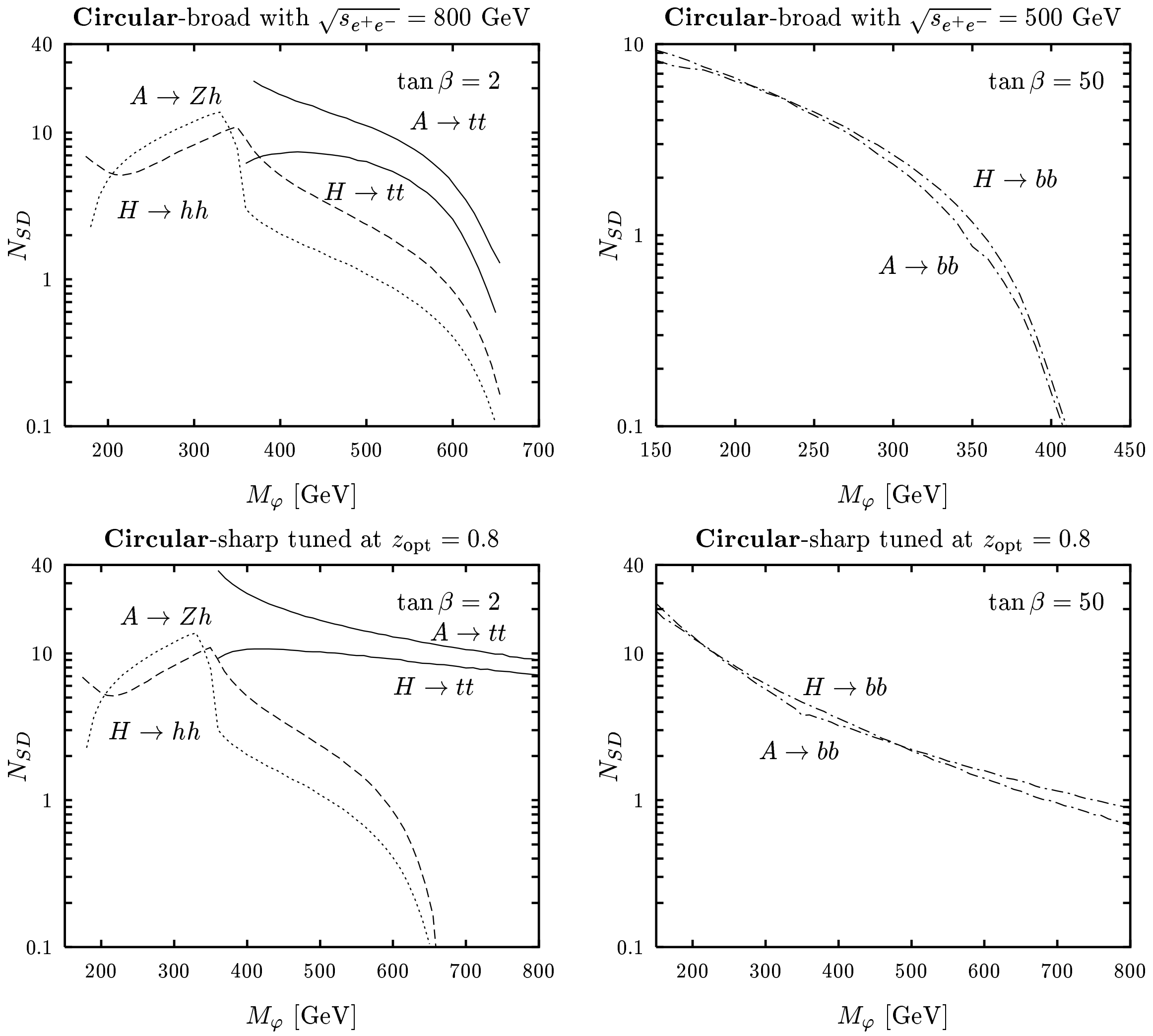

Figure 6: Statistical significance, N_{SD}, of the H and A signals for $L_{\rm eff} = 100$ fb^{-1} in the two modes of operation of the PLC with circular laser polarizations, for $t\bar{t}$ (solid), $b\bar{b}$ (dot-dashed), hh (dashed) and Zh (dotted) final states.

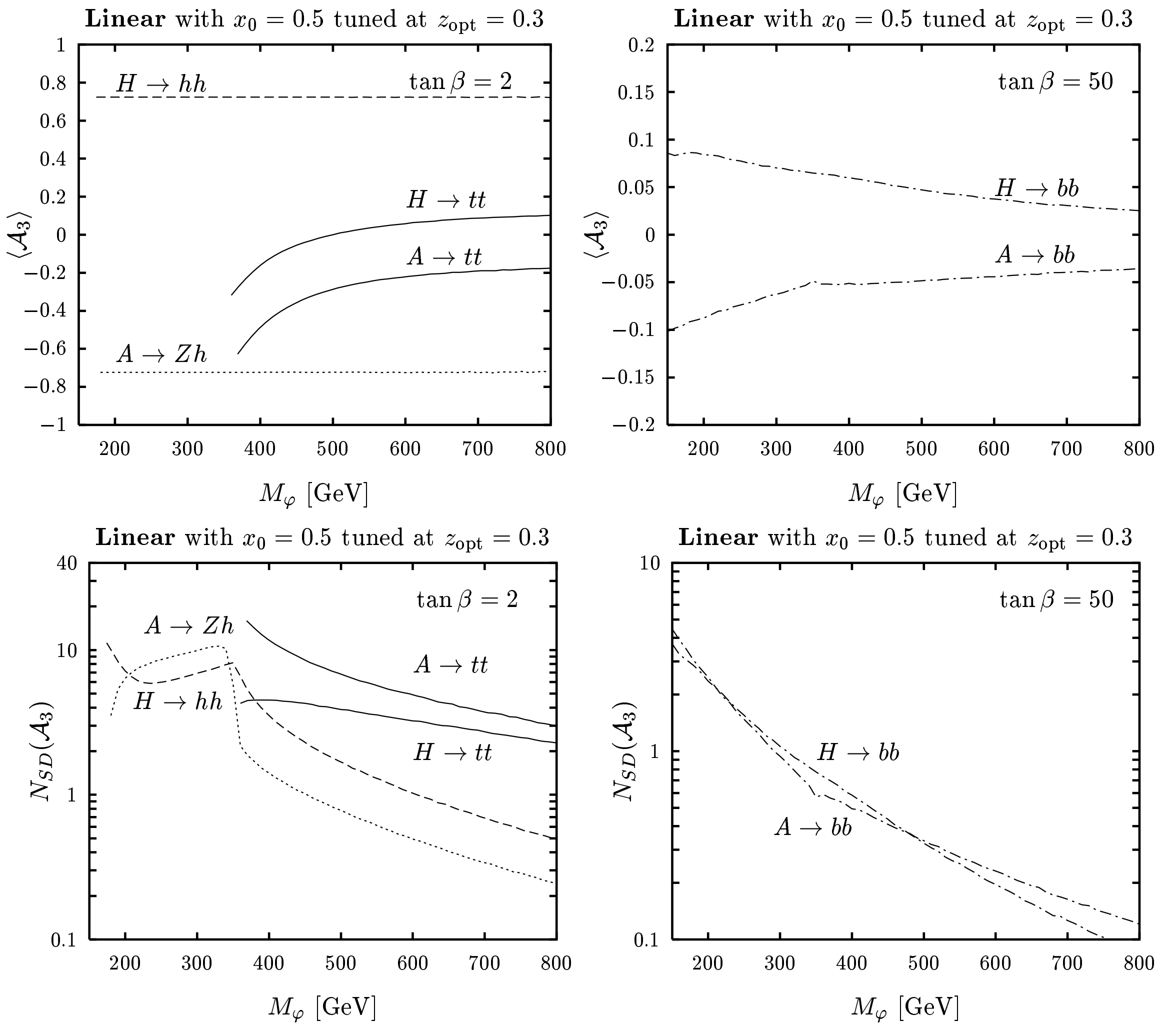

Figure 7: The expectation value of the asymmetry $\mathcal{A}_3$ and its statistical significance ($L_{\rm eff} = 100$ fb^{-1}) for the PLC operating with linear polarizations at a tuned energy with $x_0 = 0.5$. The final states are labelled as before: $t\bar{t}$ (solid), $b\bar{b}$ (dot-dashed), hh (dashed) and Zh (dotted).

the background. The induced polarizations of the Compton photons are shown in Fig. 2. We take fully polarized lasers, $\boldsymbol{\lambda_e} = \tilde{\boldsymbol{\lambda}}_{\boldsymbol{e}} = 0.85/2$ and a realistic interaction region with $\rho = 0.6$.

For the channels $H \to hh$ and $A \to Zh$, considered to be free of background, the asymmetries are maximal: $\langle \mathcal{A}_3^\varphi \rangle = \eta_{\rm CP}^\varphi \cdot 0.72$ (0.45) for $x_0 = 0.5$ (1.0), respectively (Figs. 7, 8).

Notice that $\langle \mathcal{A}_3 \rangle$ does not vanish in absence of a signal. Furthermore, the background contribution to the asymmetry from $q\bar{q}$ final states is always *negative* (29), since $\hat{\tau} = \hat{\sigma}_{||} - \hat{\sigma}_{\perp} < 0$, although it is negligible very far from threshold ($b\bar{b}$ and $c\bar{c}$ pairs). For the $t\bar{t}$ channel the situation is different (see Fig.4) and $\mathcal{A}_3$ has even "wrong" sign for $M_H \lesssim 500$ GeV. In any case, the presence of background reduces the absolute value of the asymmetry due to the increase of the denominator of (31). The use of like-handed linac beams helps to somewhat control the typically large $J_z = \pm 2$ component of the background, but the necessary choice of a small x_0 makes it less efficient in comparison to the case of maximal $x_0 = 4.83$ and circularly polarized lasers, discussed in the previous Section.

The statistical significance of the CP-asymmetry is given by [15]

$$N_{SD}(\mathcal{A}_3^\varphi) = \frac{|\sigma_{\rm eff}^\varphi(\Delta\gamma = 0) - \sigma_{\rm eff}^\varphi(\Delta\gamma = \pi/2)|}{\sqrt{\sigma_{\rm eff}(\Delta\gamma = 0) + \sigma_{\rm eff}(\Delta\gamma = \pi/2)}} \sqrt{L_{\rm eff}}. \tag{33}$$

Two runs with different laser polarizations are necessary. We take, for definiteness, a somewhat optimistic $L_{\rm eff} = 100$ pb^{-1} per run. The linac and laser energies are tuned for these analyses so that the Higgs bosons sit at $z_{\rm opt}$ for a given value of x_0. We presume that the Higgs mass(es) will be known by some other means, so that such tuning is possible, and that the laser and linac can reach the demanded energies available (see Eqs. 15, 16). Taking $x_0 = 1.0$ one can get 50% larger Higgs boson masses than with $x_0 = 0.5$, but then smaller asymmetries are obtained. Nevertheless, the statistical significances do not improve very dramatically for the smaller x_0 (compare Fig. 7 with Fig. 8).

A clear distinction of the CP-parity of the heavy MSSM Higgs bosons is possible for the low $\tan\beta$ scenario in the whole range of accessible masses of the photon collider, based on tunable linac and lasers ($M_\varphi \leq 450$ GeV for $\sqrt{s_{e^+e^-}} \leq 1$ TeV). Below the top-pair threshold, the CP-even (-odd) Higgs bosons decay into light-Higgs pairs hh (or Zh, respectively), and for heavier Higgs bosons, into top pairs. The signal, particularly for the pseudoscalar, is very clear in the low $\tan\beta$ scenario. If $\tan\beta$ happens to be large, the bb decay channel is favoured, and the CP-asymmetry allows to distinguish the CP-parity only if the Higgs bosons are lighter than ~ 300 GeV, since the background-suppression power of this collider configuration is not so efficient as with circularly polarized lasers. The signals are not so large as in the small $\tan\beta$ case either.

Testing the CP-parity of h is also feasible. A light Higgs boson decays mostly into $b\bar{b}$ pairs. One can choose a small $x_0 = 0.5$ and tune the collider at $z_{\rm opt} = 0.45$ to cover the whole range of possible masses [$M_h \lesssim 100$ (130) GeV for low (high) $\tan\beta$], for which a maximal $\sqrt{s_{e^+e^-}} \sim 250$ GeV is needed. Statistical significances for the CP asymmetry of more than one standard deviation are obtainable [15].

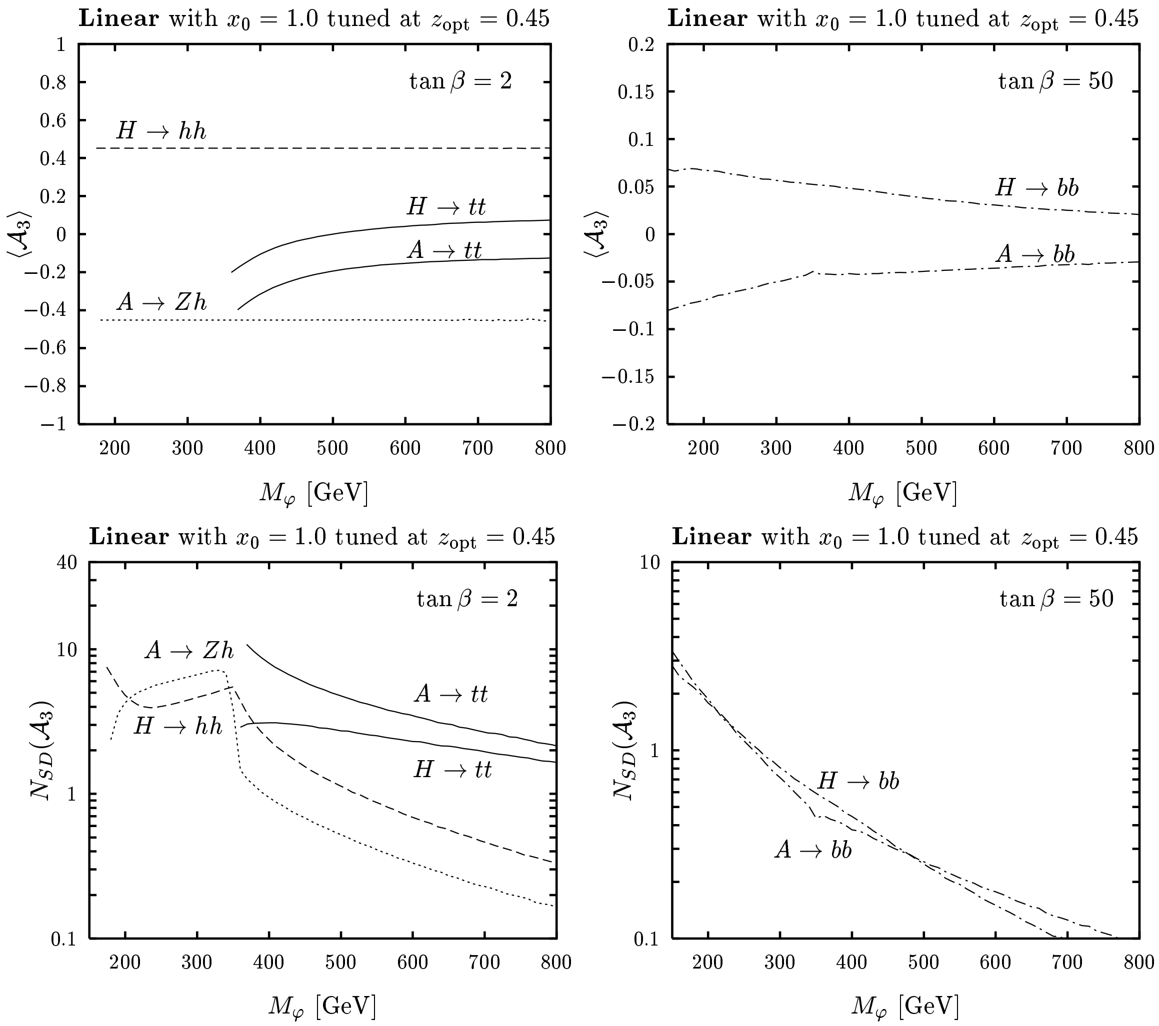

Figure 8: The same as in Fig. 7 but with $x_0 = 1.0$

7 Conclusions

We have presented a self-contained introduction to the phenomenology of a high energy photon collider, including a derivation of the $\gamma\gamma$ luminosity spectra with especial emphasis on the polarization effects and their influence on the resonant Higgs production and decay, as well as on the most relevant backgrounds.

We have explored the photon-collider potential to observe and test the CP-parity of the heavy neutral MSSM Higgs bosons.

With circularly polarized lasers one can maximally profit from the linear collider energy and, at the same time, very efficiently reduce the $J_z = \pm 2$ component of the continuum background, by choosing an extreme value of $x_0 \equiv 4\omega_0 E_b/m_e^2 \approx 2(1+\sqrt{2})$. For fixed linac and laser energies (E_b and ω_0, respectively) and like-handed lasers and electrons or, even better, using opposite-handed electrons and lasers for both arms of the collider and tuning the linac energy to the luminosity peak, heavy Higgs bosons with masses below 800 GeV can be observed in a linear collider tunable up to $2E_b = 1$ TeV. The tuned-energy option, but at more moderate energies, is also the best configuration to produce an intermediate-mass Higgs boson and measure its two-photon width with very good accuracy [9].

In the low $\tan\beta$ scenario, and below the top-pair threshold, H can be observed to decay into hh and A into Zh, but for heavier Higgs bosons the $t\bar{t}$ final state is best, with a larger rate for the pseudoscalar. In the high $\tan\beta$ scenario the $b\bar{b}$ channel is common to both at a similar, but smaller rate than for low $\tan\beta$.

To determine the CP-parity of the Higgs bosons, laser linear polarizations are absolutely necessary. The CP-even (CP-odd) Higgs bosons couple only to two photons with parallel (orthogonal) polarizations. Samples rich in those initial states can be prepared by choosing a smaller x_0 at the price of a smaller Higgs-mass reach $M_\varphi \propto x_0/(x_0+1)$. A longitudinal polarization of the linac beams helps to suppress the background, although less efficiently than in the case of circular laser polarizations. An asymmetry based on the comparison of production rates for parallel and perpendicular laser-polarization planes allows a clear distinction of H and A. The CP-parity of Higgs bosons with masses below ~450 (300) GeV can be tested in the low (high) $\tan\beta$ region with a photon collider based on a linac tunable up to 1 TeV.

Acknowledgements

I am very grateful to A. Djouadi for suggestions and comments, to A. Schiller and V. Serbo for a helpful communication and to T. Riemann and A. Tkabladze for discussions. I also thank A. Djouadi, M. Jack, T. Riemann and A. Tkabladze for carefully reading the manuscript. This work has been partially supported by the Spanish CICYT and Junta de Andalucía, under contracts AEN96-1672 and FQM101, respectively.

References

[1] The LEP Collaborations, the LEP Electroweak Working Group, and the SLD Heavy Flavour and Electroweak Working Groups, CERN-EP/99-15.

[2] For a recent review on Higgs bosons, see e.g. J.F. Gunion, in Perspectives on Higgs Physics (to appear), ed. G.L. Kane, 2nd edition (World Scientific Publishing), hep-ph/9705282.

[3] J.F. Gunion, H.E. Haber, G.L. Kane, and S. Dawson, *The Higgs Hunter's Guide*, Addison-Wesley, Reading, 1990.

[4] M. Carena, S. Heinemeyer, C.E.M. Wagner, and G. Weiglein, hep-ph/9912223.

[5] The LEP Working Group for Higgs Boson Searches, CERN-EP/99-060.

[6] A. Djouadi, V. Driesen, W. Hollik, and J.I. Illana, Eur. Phys. J. **C1** (1998) 149.

[7] I.F. Ginzburg, G.L. Kotkin, V.G. Serbo, and V.I. Telnov, Pizma ZhETF **34** (1981) 514; JETP Lett. **34** (1982) 491; Nucl. Instrum. Meth. **A205** (1983) 47.

[8] D.L. Borden, D.A. Bauer, and D.O. Caldwell, Phys. Rev. **D48** (1993) 4018.

[9] G. Jikia and S. Söldner-Rembold, hep-ph/9910366.

[10] I.F. Ginzburg, G.L. Kotkin, S.L. Panfil, V.G. Serbo, and V.I. Telnov, Nucl. Instrum. Meth. **A219** (1984) 5.

[11] I.G Ginzburg and G.L. Kotkin, hep-ph/9905462.

[12] V.I. Telnov, Nucl. Instrum. Meth. **A294** (1990) 72.

[13] V.I. Telnov, Nucl. Instrum. Meth. **A335** (1995) 3.

[14] G.L. Kotkin and V.G. Serbo, Phys. Lett. **B413** (1997) 122.

[15] J.F. Gunion and J.G. Kelly, Phys. Lett. **B333** (1994) 110.

[16] ECFA/DESY LC Physics Working Group, E. Accomando et al., Phys. Rep. **299** (1998) 1;
R. Brinkmann, G. Materlik, J. Rossbach and A. Wagner (eds.), *Conceptual Design Report of a 500 GeV e+e- Linear Collider with Integrated X-ray Laser Facility*, DESY 1997-048, ECFA 1997-182, `http://www.desy.de/~schreibr/cdr/cdr.html`;
R. Brinkmann at al., *An interaction region for gamma gamma and gamma electron collisions at TESLA/SBLC*, Nucl. Instrum. Meth. **A406** (1998) 13 (also in DESY-97-048, App. A, p. 1089).

[17] B. Grządkowski and J.F. Gunion, Phys. Lett. **B294** (1992) 361.

[18] S.Y. Choi and J.S. Lee, hep-ph/9912330.

[19] A. Djouadi, J. Kalinowski, and M. Spira, Comput. Phys. Commun. **108** (1998) 56.

[20] A. Djouadi, J. Kalinowski, and P.M. Zerwas, Z. Phys. **C70** (1996) 435;
M. Spira, Fortschr. Phys. **46** (1998) 203.

[21] S.H. Zhu, C.S. Li, and C.S. Gao, Phys. Rev. **D58** (1998) 015006.

[22] M. Drees, M. Krämer, J. Zunft, and P.W. Zerwas, Phys. Lett. **B306** (1993) 371;
J.H. Kühn, E. Mirkes, and J. Steegborn, Z. Phys. **C57** (1993) 615;
D.L. Borden, V.A. Khoze, J. Ohnemus, and W.J. Stirling, Phys. Rev. **D5** (1994) 4499;
B. Kamal, Z. Merbashvili, and A.P. Contogouris, Phys. Rev. **D51** (1995) 4808;
G. Jikia and A. Tkabladze, Phys. Rev. **D54** (1996) 2030;
M. Melles, W.J. Stirling, and V.A. Khoze, DTP-99-70, hep-ph/9907238.

[23] A. Denner, S. Dittmaier, and M. Strobel, Phys. Rev. **D53** (1996) 44.

[24] G. Jikia and A. Tkabladze, work in preparation.

[25] E. Asakawa, J. Kamoshita, A. Sugamoto, and I. Watanabe, hep-ph/9912373.

[26] M. Krämer, J. Kühn, M.L. Stong, and P.M. Zerwas, Z. Phys. **C64** (1994) 183.

[27] A. Djouadi, M. Spira, and P.M. Zerwas, Phys. Lett. **B311** (1993) 255.